Structure−Property Relations in Multiferroic [(CH₃)₂NH₂]M(HCOO)₃ (M = Mn, Co, Ni)

Kendall D. Hughey,[†] Amanda J. Clune,[†] Michael O. Yokosuk,[†] Jing Li,[‡,¶] Nandita Abhyankar,[§,‖] Xiaxin Ding,[⊥] Naresh S. Dalal,[§,‖] Hongjun Xiang,[‡,¶] Dmitry Smirnov,[§] John Singleton,[⊥] and Janice L. Musfeldt*[†,#]

[†]Department of Chemistry, University of Tennessee, Knoxville, Tennessee 37996, United States

[‡]Key Laboratory of Computational Physical Sciences (Ministry of Education), State Key Laboratory of Surface Physics and Department of Physics, Fudan University, Shanghai 200433, People's Republic of China

[¶]Collaborative Innovation Center of Advanced Microstructures, Nanjing 210093, People's Republic of China

[§]National High Magnetic Field Laboratory, Tallahassee, Florida 32310, United States

[‖]Department of Chemistry and Biochemistry, Florida State University, Tallahassee, Florida 32306, United States

[⊥]National High Magnetic Field Laboratory, Los Alamos National Laboratory, Los Alamos, New Mexico 87545, United States

[#]Department of Physics, University of Tennessee, Knoxville, Tennessee 37996, United States

ABSTRACT: We bring together magnetization, infrared spectroscopy, and lattice dynamics calculations to uncover the magnetic field-temperature (*B-T*) phase diagrams and vibrational properties of the [(CH₃)₂NH₂]M(HCOO)₃ (M = Mn²⁺, Co²⁺, Ni²⁺) family of multiferroics. While the magnetically driven transition to the fully saturated state in [(CH₃)₂NH₂]Mn(HCOO)₃ takes place at 15.3 T, substitution with Ni or Co drives the critical fields up toward 100 T, an unexpectedly high energy scale for these compounds. Analysis of the infrared spectrum of the Mn and Ni compounds across T_C reveals doublet splitting of the formate bending mode which functions as an order parameter of the ferroelectric transition. By contrast, [(CH₃)₂NH₂]Co(HCOO)₃ reveals a surprising framework rigidity across the order−disorder transition due to modest distortions around the Co²⁺ centers. The transition to the ferroelectric state is thus driven by the dimethylammonium cation freezing and the resulting hydrogen bonding. Under applied field, the Mn (and most likely, the Ni) compounds engage the formate bending mode to facilitate the transition to their fully saturated magnetic states, whereas the Co complex adopts a different mechanism involving formate stretching distortions to lower the overall magnetic energy. Similar structure−property relations involving substitution of transition-metal centers and control of the flexible molecular architecture are likely to exist in other molecule-based multiferroics.
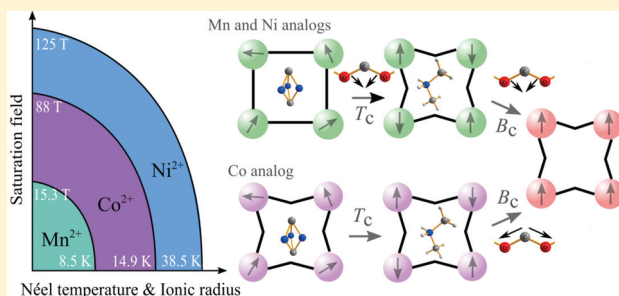
INTRODUCTION

Multiferroics are fascinating materials where ferroelectric and magnetic orders coexist, and spatial-inversion and time-reversal symmetries are simultaneously broken.[1−4] They are also potential platforms for the development of ultralow-power memory, switching devices, and novel computing architectures.[5] The most well-studied multiferroics, for instance BiFeO₃, EuTiO₃, and the rare-earth manganites, are oxides with perovskite-like structures.[6−8] Recently, molecule-based multiferroics have attracted attention. Though their transition temperatures are not as large as those of the oxides and related superlattices[9] and the coupling between their polarization and magnetization is smaller, they offer energy scales that are well matched to convenient laboratory fields and temperatures, along with flexible molecular architectures, easily varied by chemical substitution.[10−13] They are therefore very convenient systems for the study of emergent properties. Many of these

materials, for instance, [CH₃NH₃][Co(HCOO)₃] and [C₂H₅NH₃][Na₀.₅Fe₀.₅(HCOO)₃], are hybrid organic−inorganic perovskites.[14,15] Others include the A₂[FeCl₅(H₂O)] (A = K, Rb, NH₄) family of erythrosiderites where cation substitution alters magnetoelectric properties,[16] perovskite-like CuCl₄(C₆H₅CH₂CH₂NH₃)₂,[10] low-symmetry organic charge-transfer salts like κ-(ET)₂Cu[N(CN)₂]Cl,[17] and even transition-metal halide monolayers such as CrBr₃.[18] Control of the counterion and metal center plus ligand substitution permit systematic exploration of structure−property relations.[16,19]

In this work, we focus on the [(CH₃)₂NH₂]M(HCOO)₃ (M = Mn²⁺, Co²⁺, Ni²⁺) family of hybrid organic−inorganic perovskites.[20] These systems possess a perovskite-like ABX₃ formula, where A is a charge-compensating cation (in this case,

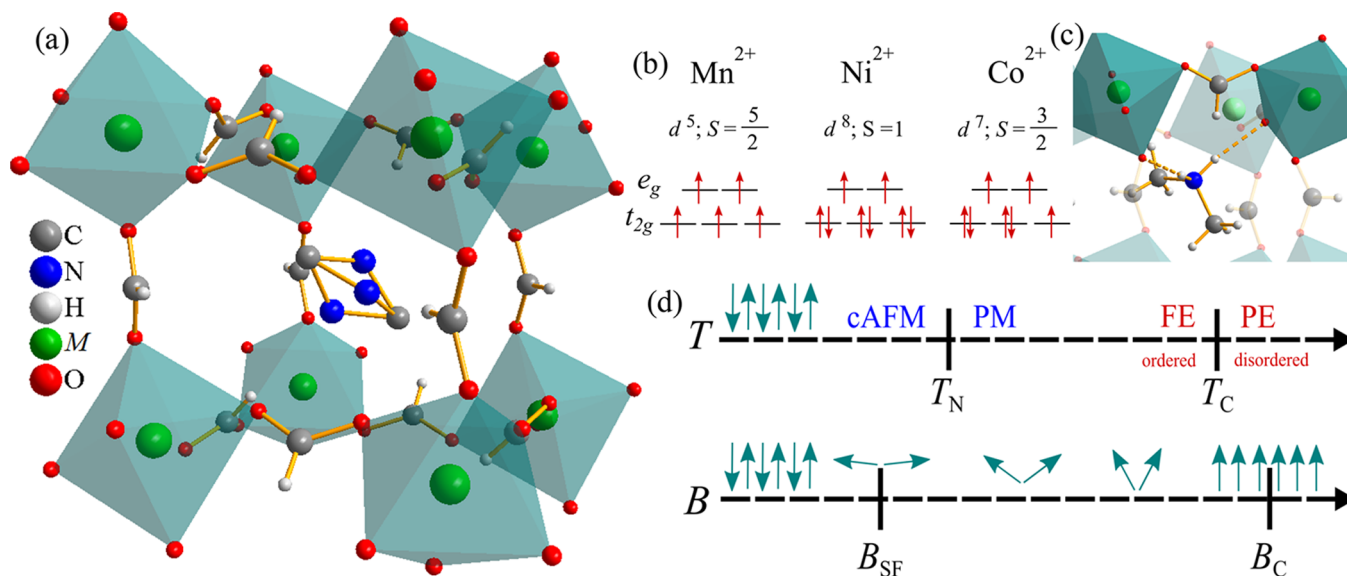**Figure 1.** (a) Crystal structure of $[(CH_3)_2NH_2]M(HCOO)_3$ showing the metal centers ($M = Mn^{2+}, Co^{2+}, Ni^{2+}$), formate ligands, and disordered dimethylammonium at room temperature.[20] (b) Comparison of electronic and spin states for the different transition-metal centers. (c) Close-up view of the counterion in the ordered low-temperature state. (d) Temperature and magnetic field energy scales showing the characteristic transitions. cAFM = canted antiferromagnet, PM = paramagnet, FE = ferroelectric, PE = paraelectric, B_{SF} = spin flop field, and B_C = saturation field.

Table 1. Comparison of Important Properties in $[(CH_3)_2NH_2]M(HCOO)_3$ ($M = Mn^{2+}, Co^{2+}, Ni^{2+}$)[a]

M^{2+}	S	T_C (K)	T_N (K)	B_{SF} (T)	B_C (T)	P ($\mu C/cm^2$)	J (K)	J (K) (DFT)
Mn	5/2	185[20]	8.5[20,26]	0.31[13]	15.3[13]	1.5[29]	−0.64[20,26]	−1.12[b]
Co	3/2	165[20]	14.9[20,26]	11.2[b]	88[b]	–	−3.2[20,26]	−3.79[b]
Ni	1	180[20]	35.6[20,26]	7.7[b]	125[b]	–	−6.79[20,26]	−24.6[b]

[a]Here, P is the polarization, J is the dominant exchange energy (calculated according to molecular field theory[26] as well as DFT), and other symbols are defined in the caption of Figure 1. Parameters measured in other works are cited. [b]Indicates values derived in the present paper.

a dimethylammonium (DMA^+) cation, $(CH_3)_2NH_2$, B is a transition metal ion, and X is a ligand that connects the metal centers (in this case, the $HCOO^-$ anion). Naturally, B-site substitution modifies the magnetic properties.[21,22] It is also a powerful tool for the enhancement of properties like ferroelectricity.[23] The Mn compound has received the most attention thus far, with its structure consisting of a cage of metal centers linked by formate ligands with a rotating dimethylammonium cation inside the cavity (Figure 1a).[20] Ferroelectricity is induced by cation ordering across $T_C = 185$ K,[20,24] and noncollinear antiferromagnetism develops below $T_N = 8.5$ K.[20,25,26] The ferroelectric transition mechanism is interesting. Hydrogen-bond development between the counterion and the framework drives the material through the order−disorder transition and into the ferroelectric state (Figure 1c). Hydrogen-bond lengths through this transition have been extensively studied with neutron scattering, revealing direct evidence of the local structure of the hydrogen bonding from the counterion to the framework and the specific distortions responsible for the phase transition.[27] Recent theoretical modeling also shows that the overall polarization is derived from the dipole moment as well as the tilting angle of the cations, creating spontaneous polar domains below T_C.[28] Another interesting aspect of the phase below T_C is the magnetic field-induced enhancement of the polarization, although there is some debate about the extent of this magnetoelectric coupling.[28−30] There is a series of transitions under a magnetic field as well. Magnetization reveals a spin flop at 0.31 T and a saturation field of 15.3 T.[13] These energy

scales are schematically summarized in Figure 1d and quantitatively tabulated in Table 1.

Less is known about the Co and Ni analogs. Data from this and other work suggest that the general character of the temperature- and magnetic-field-driven transitions are similar, although the exact values of T_C, T_N, B_{SF}, and B_C vary depending on the identity of the metal center. Table 1 summarizes these values. In $[(CH_3)_2NH_2]Co(HCOO)_3$, the magnetic moment also changes across T_C, suggesting a modification of the spin state at the ferroelectric transition.[31] This is not seen in the other analogs.[31] The Co compound also exhibits glassy magnetism due to magnetic phase coexistence near $T_N = 14.9$ K.[25,32] Detailed vibrational mode assignments have been proposed for the Ni compound, and dielectric and magnetization measurements reveal signatures of the transitions.[20,33]

In this work, we bring together high field techniques, magnetization, and infrared spectroscopy to reveal the structure−property relations associated with B-site substitution in the $[(CH_3)_2NH_2]M(HCOO)_3$ family of materials. In addition to uncovering the magnetic field-temperature phase diagrams, we unravel the microscopic details of the mechanisms involved in the development of ferroelectricity and the fully saturated magnetic state. The Mn and Ni complexes are overall quite similar, despite their large energy scale differences, whereas the Co analog displays strikingly different mechanisms in the development of polarization and the fully saturated magnetic state. These differences largely arise from distortions of the CoO_6 octahedra. Taken together,
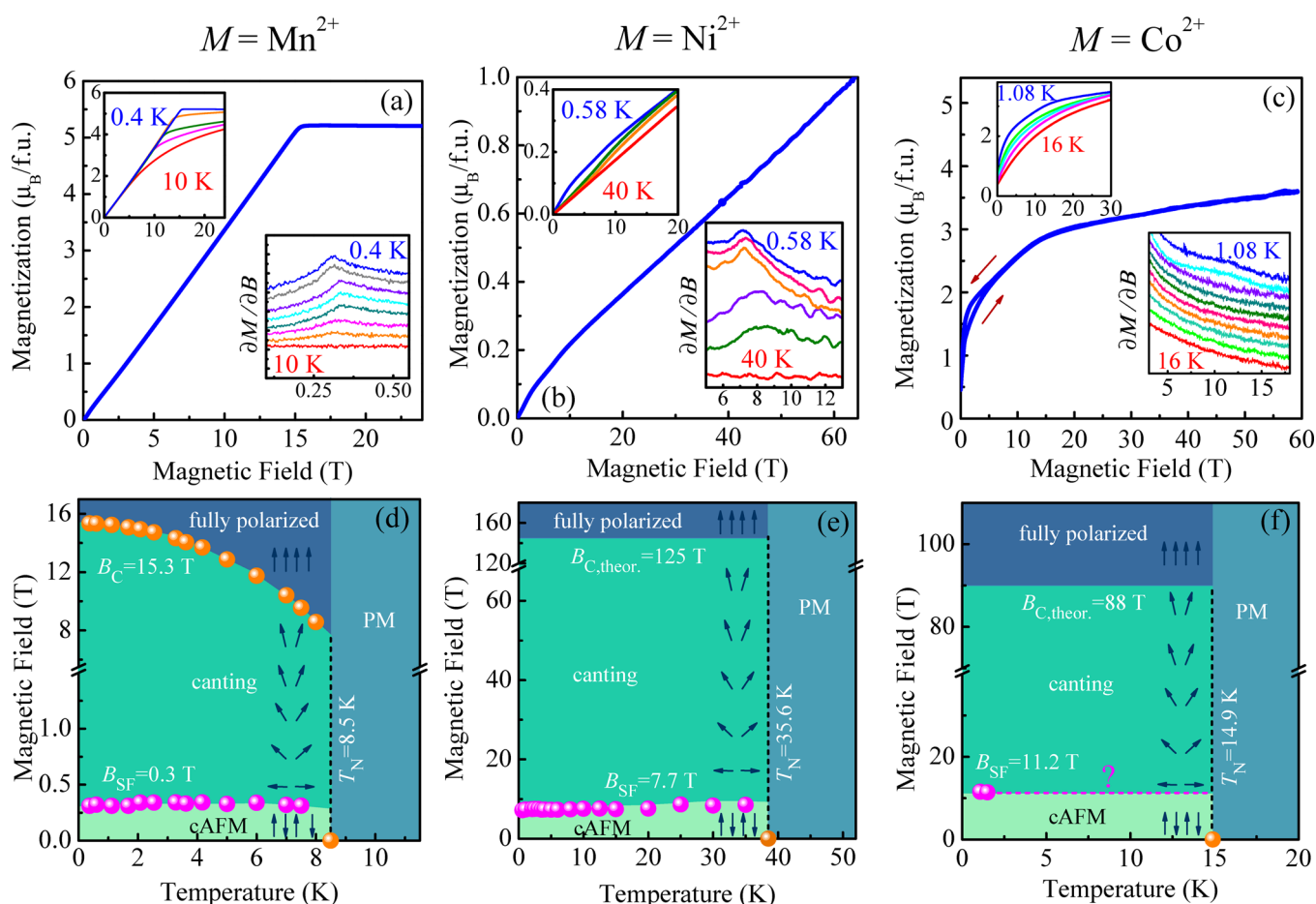
Figure 2. (a−c) Pulsed field magnetization of $[(CH_3)_2NH_2]M(HCOO)_3$ (M = Mn²⁺, Co²⁺, Ni²⁺) up to 65 T at different temperatures. Derivatives of this data reveal B_{SF} as shown in the lower insets. Only the Mn compound has a clear saturation field under these conditions.[13] The Ni and Co systems are not saturated even at 65 T. (d−f) Magnetic field-temperature phase diagrams developed from the pulsed field magnetization data. Orange points denote the transition to the fully saturated magnetic state, and pink points indicate the spin flop. The high field phase boundaries for the Ni and Co compounds are estimated as described in the text. Error bars are on the order of the symbol size. cAFM = canted antiferromagnet, and PM = high-temperature paramagnetic state.

these findings reveal that B-site substitution is a powerful tool for the control of magnetic energy scales and the mechanisms that underlie ferroelectricity and magnetism.

■ MATERIALS AND METHODS

Single and polycrystalline samples of $[(CH_3)_2NH_2]M(HCOO)_3$ (M = Mn²⁺, Co²⁺, Ni²⁺) were grown by solvothermal techniques[20] and mixed with paraffin or KBr for transmittance in the far and middle infrared, respectively. Use of a matrix provides for isotropic compression and allows control of optical density. Grain sizes were on the order of 10 μm. High field magnetization measurements were performed on polycrystalline samples at the National High Magnetic Field Laboratory using the 65 T short-pulse magnet as described previously.[13] Controlled temperatures down to 0.4 K were provided using a ³He cryostat. A Quantum Design PPMS was used to benchmark magnetic moments for each material. A series of Fourier-transform spectrometers and an open flow cryostat system were employed for variable-temperature infrared spectroscopy (20−5000 cm⁻¹; 4.2−300 K). Absorption was calculated as $\alpha(\omega) = -\frac{1}{hd}\ln(\mathcal{T}(\omega))$, where $\mathcal{T}(\omega)$ is the measured transmittance, h is the concentration, and d is the thickness. Temperature ramp rates were on the order of 0.2 K/min. Magneto-infrared measurements were performed at the National High Magnetic Field Laboratory at 4.2 K using a 35 T resistive magnet. Absorption differences were calculated as $\Delta\alpha = \alpha(\omega,B) - \alpha(\omega,B=0)$ in order to emphasize small changes with magnetic field. We quantify effects for particular

phonons of interest by integrating the absolute value of $\Delta\alpha$ over a small energy window and plotting these differences vs applied field. This procedure gives trends that follow the field-induced frequency shift, but with a lot less noise.[34] Traditional peak fitting techniques were also employed as appropriate.[35] Structural relaxations, energies, and lattice dynamics calculations were performed using density functional theory (DFT) plus the on-site repulsion (U) method[36,37] as implemented in VASP[38,39] to reveal mode assignments and displacement patterns. The on-site and nearest-neighbor repulsion (V) are set to standard values of 4 and 1 eV for Co, respectively.[40] The electron−ion interactions were treated using the projected augmented wave method.[41,42]

■ RESULTS AND DISCUSSION

Developing Magnetic Field-Temperature Phase Diagrams. Figure 2a−c displays the pulsed field magnetization for the $[(CH_3)_2NH_2]M(HCOO)_3$ (M = Mn²⁺, Co²⁺, Ni²⁺) family of materials.[43] The Mn system sports a 0.31 T spin flop transition, and the magnetization rises linearly until it saturates at 15.3 T.[13] This value of B_C is consistent with J = 0.64 K;[13,20,26] materials with such low magnetic energy scales can be fully polarized by moderate laboratory fields. The critical field for saturation is a sharply defined feature in the magnetization at 0.4 K that broadens as the temperature approaches T_N. Above T_N = 8.5 K, there is no evidence for the spin flop, and
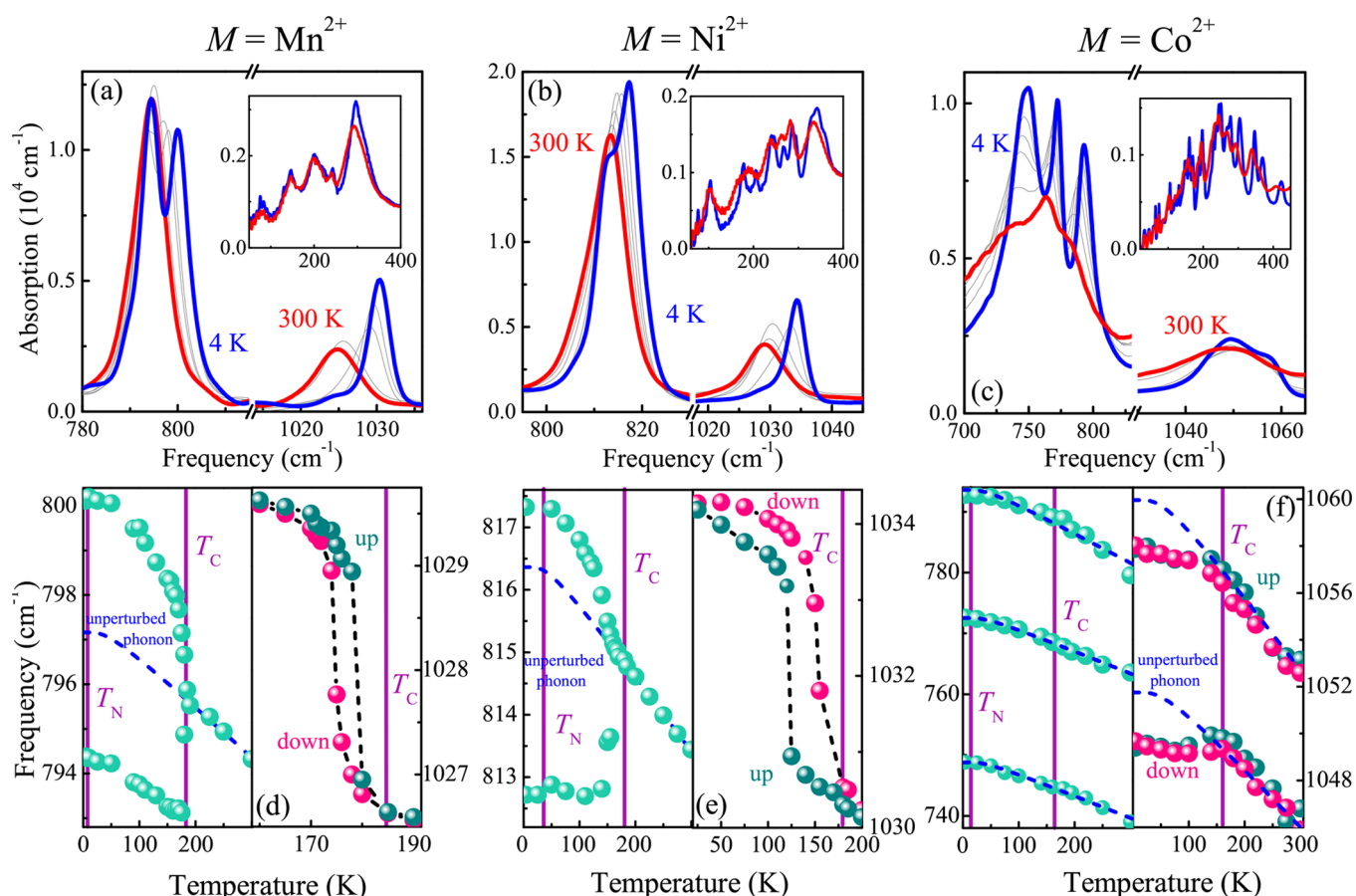
Figure 3. (a−c) Close-up views of the formate bending mode (left) and C−N−C stretch (right) for the Mn, Ni, and Co analogs as a function of temperature. Insets show low frequency modes. (d−f) Frequency vs temperature plots for these features, highlighting the difference in behavior of the Mn and Ni complexes vs the Co system. T_C and T_N are indicated by purple vertical lines. The fit to the high-temperature phase data described in the text represents the behavior of the hypothetical unperturbed phonons below T_C.

the approach to saturation is much more gradual—both consequences of fluctuating regions of short-range order as opposed to the long-range order that occurs at low temperatures.[44]

The distinctive high field behavior of multiferroic $[(CH_3)_2NH_2]Mn(HCOO)_3$ motivated our extension to the Co and Ni analogs.[13,14,45] Just as in $[(CH_3)_2NH_2]Mn(HCOO)_3$, the Ni and Co systems display spin-flop transitions, but at higher fields of 7.7 and 11.2 T, respectively (insets, Figure 2b,c). The signature of the spin flop in the Co system is subtle and is only seen in the magnetization at the lowest temperatures. We also searched for saturation in the Ni and Co compounds; however, even 65 T fails to saturate the magnetization of these materials (Figure 2b,c). Simple metal site substitution therefore alters the overall energy scales significantly.

In order to generate magnetic field-temperature phase diagrams for these materials, we tracked B_{SF} and, where feasible, B_C as a function of temperature. First derivatives, $\partial M/\partial B$, were used to better highlight the positions of the features in $M(B)$.[13] Figure 2d−f summarizes our results. The behavior of the Mn analog is representative of a classic antiferromagnet, where magnetic field drives the system across a low-field spin-flop transition and into the fully saturated magnetic state at 15.3 T.[13,46] The magnetic field-temperature phase diagrams for the Ni and Co complexes reveal a similar story albeit with higher energy scales. The latter is evident in both the size of

B_{SF}[47] and the fact that 65 T does not saturate the magnetization. We can estimate the saturation fields for the Co and Ni compounds by equating the total exchange energies from Table 1 to the total Zeeman energy via the Hamiltonian $H = -zJ\sum S_i \cdot S_j - g\mu_B B_C \sum S_i^z$ ($z = 6$, $g = 2.0$, $S = 1$ for Ni and $S = 3/2$ for Co).[30] We find $B_C = 125$ T and $B_C = 88$ T for the Ni and Co analogs, respectively. Alternatively, we can estimate B_C by extrapolating the linear character of $M(B)$ until it reaches magnetic saturation (defined by $g\mu_B S$) or by extrapolating the derivative of the magnetization curve down to the magnetic field axis. The critical fields obtained from this approach are in reasonable agreement with those estimated above ($B_{C,Ni} = 135$ T, $B_{C,Co} = 90$ T), validating the J values displayed in Table 1 and revealing that a spin-only approximation is reliable in these materials, at least within our error bars. These fields are significantly higher than the 15.3 T required to saturate the Mn complex. The energy scales generally follow trends in T_N as well. We therefore see that while metal substitution does not alter the overall space group of the material, there are significant local lattice distortions around the metal centers that modify superexchange interactions and magnetic energy scales.[48] These site-symmetry differences are discussed below. Similar energy scale effects can be seen in other materials like $M[N(CN)_2]_2$ (M = Mn, Co).[46,49]

Vibrational Properties of This Family of Hybrid Organic−Inorganic Perovskites Across the Ferroelectric Transition. The vibrational properties of $[(CH_3)_2NH_2]Mn-$
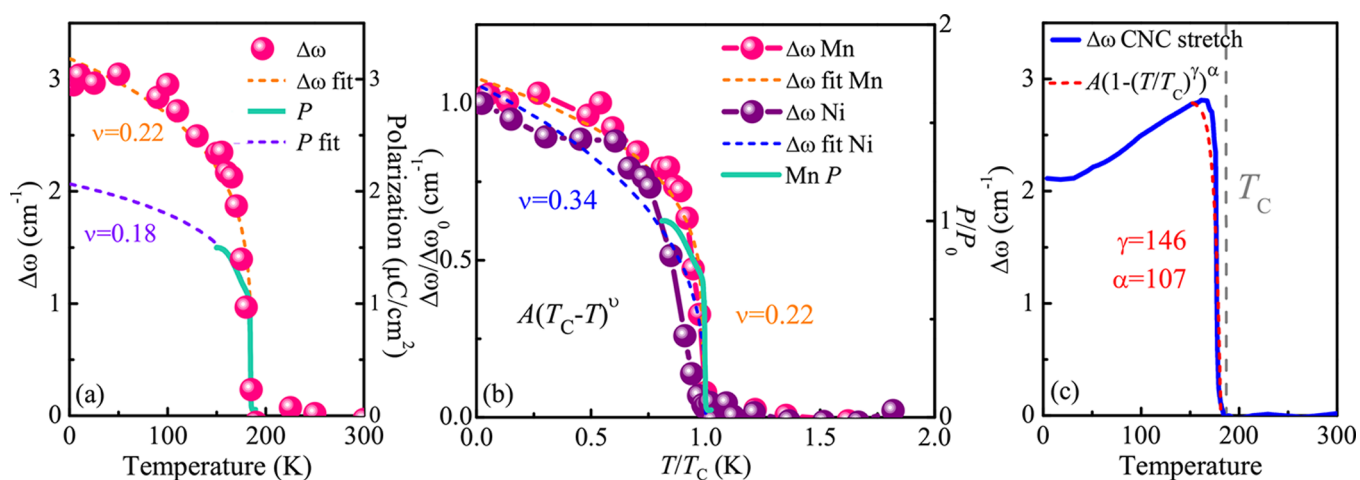
Figure 4. (a) Splitting of the formate bending mode vs temperature in the Mn complex, a power law fit to this data, and polarization from ref 29, along with a corresponding power law fit. (b) Overlay of the formate bending mode splittings in the Mn and Ni complexes, along with their power law fits and extracted critical exponents. (c) Calculated cooling rate of the C−N−C stretch along with an extended power law fit.

$(HCOO)_3$ are complex, just like many other molecule-based multiferroics, and have been the subject of numerous investigations.[24,33,50−55] Group theory predicts 32 infrared-active modes with both A_{2u} and E_u symmetries. Despite the large number of modes, only a few are useful for revealing changes at the ferroelectric transition or across the critical fields.

Figure 3a−c summarizes the behavior of two important vibrational modes of the $[(CH_3)_2NH_2]M(HCOO)_3$ (M = Mn^{2+}, Co^{2+}, Ni^{2+}) family of materials. Here, we focus on the symmetric formate bending mode near 800 cm^{-1} and the asymmetric C−N−C counterion stretch near 1030 cm^{-1}. The former links the electronic and magnetic ferroicities in the Mn complex,[35] whereas the latter is quite sensitive to amine hydrogen bonding and hysteresis effects. Peak position vs temperature plots (Figure 3d−f) demonstrate strong similarities between the Mn and Ni complexes and, at the same time, uncover distinct behavior in the Co compound.

Doublet splitting of the formate bending modes across T_C is one of the most interesting signatures of the ferroelectric transition in the Mn[13] and Ni analogs. This distortion is due to the development of two unique N−H⋯O hydrogen-bonded pathways between the counterion and the framework.[35] At base temperature, splitting in the Mn (5.7 cm^{-1}) and Ni (3.9 cm^{-1}) complexes is similar. We fit temperature trends in the paraelectric state as $\omega = \omega_0 + \Delta(T)$, where $\Delta(T) = C\left[1 + \frac{2}{e^x - 1}\right]$ with $x = \hbar\omega_0/2k_BT$. Here, ω_0 is the unperturbed phonon frequency at base temperature, $\hbar$ is the reduced Plank's constant, and k_B is Boltzmann's constant. This fit quantifies anharmonicity in the high-temperature state, and by extending it into the ferroelectric phase, we reveal how the formate bending mode would have behaved in the absence of the transition. As discussed below, doublet splitting of this mode acts as an order parameter for the ferroelectric transition in the Mn and Ni materials.

Figure 4a shows a comparison of the difference in splitting between the high-frequency branch of the formate mode in the Mn complex and the anharmonic fit, overlain with polarization measurements.[29,35] The critical exponent extracted from a power-law fit of $A(T_C-T)^\nu$ to the phonon splittings is in reasonable agreement with a fit to the polarization ($\nu = 0.22$ vs 0.18, respectively). For the power law fit to the spectroscopic

data, the entire temperature range below T_C was included; no significant change in the critical exponent was found by varying the temperature window. We also fit the available temperature range of the polarization data.[29] Here, T_C was not used as a fit parameter; this value was taken directly from ref 20. These values are suggestive of a quasi-two-dimensional system, since the total critical exponent (ν) for a true Ising system is 0.125.[56] A summary of these values is given in Table 2. Figure 4b

Table 2. Comparison of Theoretical[56] Critical Exponents ν for the Power Law Fit $A(T_C - T)^\nu$ along with Exponents Extracted from the Mn and Ni Data^a

theoretical ν		experimental ν	
mean field	0.5[56]	$[(CH_3)_2NH_2]Mn(HCOO)_3$ vibrational properties	0.22 ± 0.01
Heisenberg	0.367[56]	$[(CH_3)_2NH_2]Mn(HCOO)_3$ polarization	0.18 ± 0.02
Ising	0.125[56]	$[(CH_3)_2NH_2]Ni(HCOO)_3$ vibrational properties	0.34 ± 0.03

^{a}The values suggest that the Mn system is more two-dimensional (being closer to the predicted Heisenberg and Ising exponents), while the Ni material is closer to the mean-field, three-dimensional predictions.

displays the frequency difference between the formate bending modes and anharmonic fits for the Mn and Ni compounds. Both axes are normalized for the purpose of comparison since T_C and splitting values vary with transition-metal identity. A power law analysis reveals that while the extracted critical exponent in the Mn complex is $\nu = 0.22 ± 0.01$, the model fit for the Ni compound produces a value of $\nu = 0.34 ± 0.03$, which is larger and much closer to mean field behavior, where ν is 0.5.[56,57] The larger exponent is also indicative of a more gradual transition into the polarized state, clear from visual examination of the data, supported too by the less complete splitting pattern in Figure 3b. B-site substitution thus reveals that although the structural and vibrational properties of the Mn and Ni complexes are nearly identical, the dimensionality of the ferroelectric phase transition develops differently and is somewhat more three-dimensional in the Ni compound.

In order to compare the behavior of the framework across T_C against that of the counterion, we analyze the C−N−C
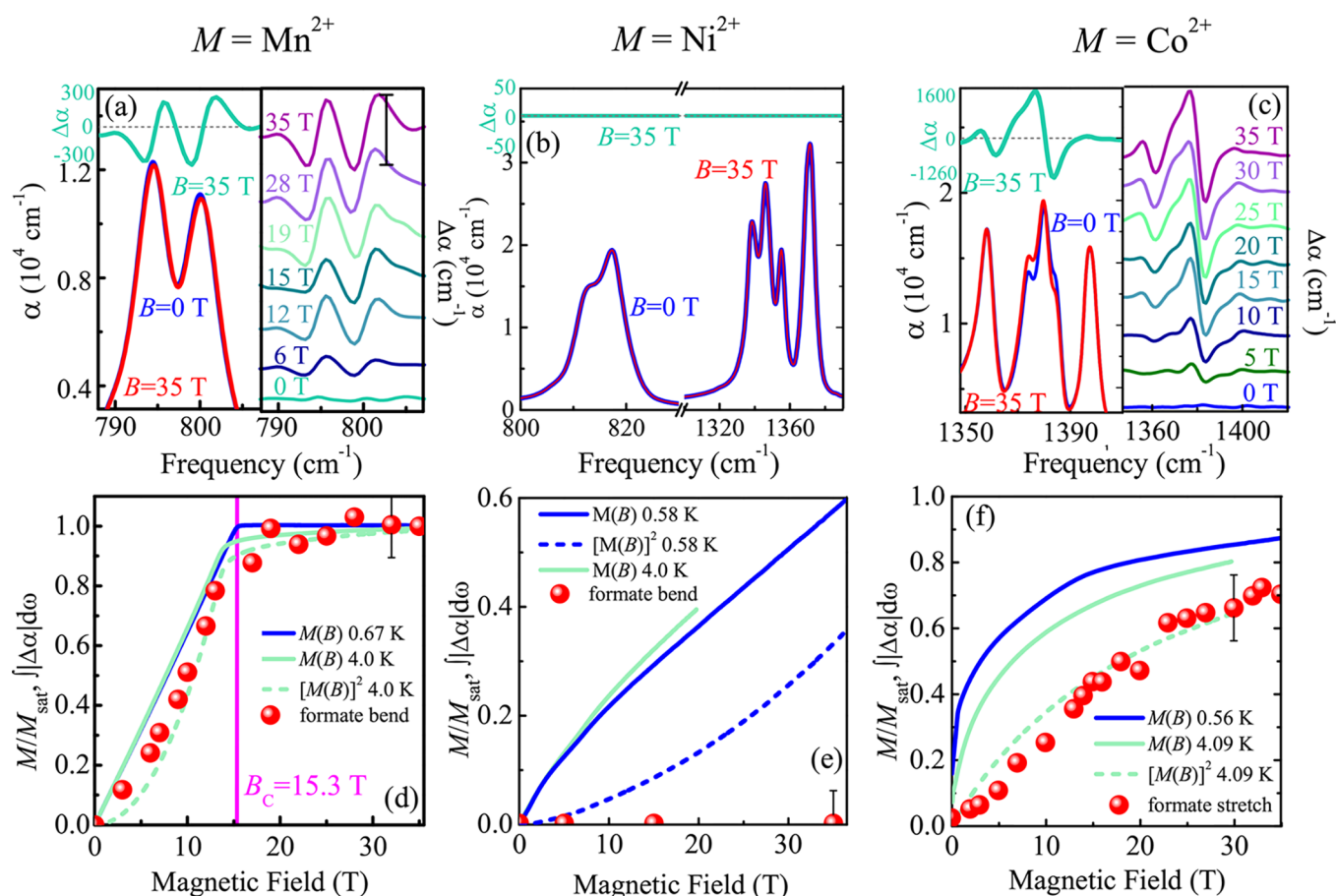
Figure 5. (a−c) Absolute absorption spectra at 0 and 35 T for the $[(CH_3)_2NH_2]M(HCOO)_3$ materials along with waterfall plots of the absorption difference at 4.2 K highlighting spectral changes in applied magnetic field. The Mn system sports field-induced changes in the formate bending mode, whereas the symmetric O−C−O stretch is important for the Co compound. The Ni analog displays no field-dependent vibrational modes up to 35 T. (d−f) Absolute value of the absorption difference integrated over a small energy window vs magnetic field along with the 4 K magnetization and the square of the magnetization. Error bars are indicated.

stretch (Figure 4c). It is well-known that the ferroelectric transition in $[(CH_3)_2NH_2]Mn(HCOO)_3$ can have a strong hysteresis. The size of the hysteresis loop is reduced with decreasing cooling rate; it collapses upon extrapolation to extremely low cooling rates.[35] An extended power law fit of $A(1 − (T/T_C)^\gamma)^\alpha$ reveals unrealistically high values of γ and α, signifying that the counterion transition is rigid and abrupt. This is evidenced by the extremely sharp step in the data (Figure 4c). Although this fit is the same form as the regular power law, the additional exponent provides extra fitting flexibility. It turns out that this makes no difference because the fit does not converge. This behavior is consistent with $(CH_3)_2NH_2$ catching slightly (due to hydrogen bonding) at T_C, distorting the structure, but then continuing to tumble within the formate framework until about 10 K below the transition temperature.[24,27] At this point, the counterion finally locks into position and the material becomes completely ordered.[24,27] Thus, the kinetics of the counterion rotation in $[(CH_3)_2NH_2]Mn(HCOO)_3$ cause the transition to be slow to relax. The delayed reaction of the amine also explains why the hysteresis curves are not centered around T_C.

The vibrational response of $[(CH_3)_2NH_2]Co(HCOO)_3$ is remarkably distinct. At room temperature, three peaks are apparent in the vicinity of the formate bend. They become increasingly resolved with decreasing temperature. A plot of peak position vs temperature reveals that these features behave

anharmonically and are completely insensitive to the development of ferroelectric polarization at T_C = 165 K (Figure 3f). This is surprising because splitting of the formate bending mode is an essential aspect of the ferroelectric transition mechanism in the Mn and Ni complexes. Where two peaks in the Mn and Ni compounds develop due to differences in hydrogen bonds from the counterion to the framework, the drive toward counterion locking is less obvious in the Co complex. We propose that this difference has its origins in slight distortions of the CoO$_6$ octahedra. This supposition is supported by our lattice dynamics calculations which predict six branches to the mode pattern. As with most materials, decreasing temperature sharpens modes by reducing line width (Figure 3c). In $[(CH_3)_2NH_2]Co(HCOO)_3$, three peaks become more resolved from the broad band with decreasing temperature. Six individual peaks are, however, not resolved due to energetic degeneracies. Although we did not notice any critical slowing down behavior, the inactivity of the framework through T_C in the Co complex is consistent with glassy character and may correlate with glassy magnetism below T_N.[25] Finally, we point out that despite the change in spin state across T_C,[31] neither the formate bending nor stretching modes engage in magneto-elastic coupling.

Figure 3d−f summarizes C−N−C counterion stretching mode behavior, which has clear features at the ferroelectric transition in all materials. In the Mn and Ni complexes, the

distortion appears as a broadened step, with the mode shifting suddenly to higher frequencies with decreasing temperature. For the same temperature–time gradient, the hysteresis loop in the Ni analog is much larger (30 K) than that in the Mn case (3 K), revealing differences in ordering speeds of the DMA^+ cation. By contrast, the C–N–C stretching mode in $[(CH_3)_2NH_2]Co(HCOO)_3$ displays a small cusp at T_C and softens upon entry into the ferroelectric state (Figure 3f). The transition does not appear to have a strong hysteresis. This mechanistic difference derives from slightly distorted CoO_6 octahedra in the room-temperature structure. In $[(CH_3)_2NH_2]Co(HCOO)_3$, the amino group locks into place quickly because the framework is already distorted, and therefore no additional distortion through T_C is required. Only the rotating counterion is important. In the Mn and Ni materials, the ferroelectric transition mechanism is a cooperative effort between the counterion and the framework, where the DMA^+ cation waits for the framework to become completely distorted before fully ordering.

Magnetoelastic Coupling and the Metal Center. Figure 5 summarizes the magneto-infrared response of our three materials of interest. As previously demonstrated, magnetoelastic coupling in $[(CH_3)_2NH_2]Mn(HCOO)_3$ involves the Mn–O–C–O–Mn superexchange pathway.[35] Evidence for this conclusion is recapped in Figure 5a,d, where the –O–C–O formate bending mode displays a derivative-like shape in $\Delta\alpha$. This is the only phonon that is sensitive to applied field. In order to demonstrate how the magneto-infrared response correlates with the spin pattern, we plot the square of the magnetization,[13] $[M(B)]^2$, and the integral of the absolute value of the absorption difference over an appropriate energy window ($\int |\Delta\alpha| d\omega$) vs magnetic field. Distortions of the formate bending mode develop with increasing field and saturate at 15.3 T, tracking $[M(B)]^2$ very well. We had anticipated that similar local lattice distortions would accompany the approach to the fully polarized magnetic transitions in the Ni and Co analogs since the mechanism for a $cAFM \rightarrow B_{SF} \rightarrow$ fully polarized state within this family of materials seems to be characteristic. We instead find substantial variations in this picture.

Figure 5b displays a close-up view of the magneto-infrared response of $[(CH_3)_2NH_2]Ni(HCOO)_3$ at 0 and 35 T in the vicinity of the formate bending and stretching modes. The full field absorption difference spectra $[\Delta\alpha = \alpha(\omega,B) - \alpha(\omega,B = 0)]$ is shown in green. The absorption difference spectra is nearly flat; in other words, there is an immeasurable difference caused by 35 T. Moreover, the full infrared spectrum was measured, and no other modes were active in field. This finding can be understood from how the B–T phase diagrams change with B-site substitution. Specifically, the Ni centers introduce a much higher energy scale than in the Mn complex (B_C = 125 T vs 15.3 T). Since the Mn and Ni behave so similarly through T_C, it is likely that the formate bending mode plays a role in the approach to magnetic saturation. This trend is not observed because an increase in magnetic energy by a factor of eight (compared to the Mn analog) is outside of our sensitivity. The overall larger energy scale in $[(CH_3)_2NH_2]Ni(HCOO)_3$ is also apparent in the spin flop fields (B_{SF} = 7.7 T vs 0.31 T).

The magneto-infrared response of $[(CH_3)_2NH_2]Co(HCOO)_3$ is shown in Figure 5c. Rather than field-induced changes in the formate bending mode, the absorption difference spectrum ($\Delta\alpha$) highlights an entirely different set of features. $\Delta\alpha$ reveals that the 1358, 1374, and 1379 cm^{-1} cluster is sensitive to magnetic field, whereas the peak at 1398 cm^{-1} is rigid. Our lattice dynamics calculations predict that the field-responsive features at 1358, 1374, and 1379 cm^{-1} are branches of the $HCOO^-$ stretch. We therefore assign these structures as formate stretching modes. Our calculations reveal that the 1379 cm^{-1} feature is different. Instead of being a formate stretch, this peak is due to a counterion vibration, in agreement with the work in ref 24. Counterion modes in other materials are also well localized and insensitive to magnetic field.[58] Although full magnetic saturation is not attained (because $B_{C,theor.}$ = 88 T and magneto-infrared spectroscopy at the National High Magnetic Field Laboratory is carried out with 35 T resistive magnets at this time), we find that $\int |\Delta\alpha| d\omega$ over the combined energy window tracks $[M(B)]^2$ very well (Figure 5f). Since these are the only modes sensitive to applied field, it is reasonable to anticipate that the distortions will cease at B_C and that the formate stretching modes are involved in the mechanisms resulting in eventual magnetic saturation. Even though the saturation field is high, field-induced spectral differences are apparent in this case because stretching modes have larger oscillator strength than bending modes, giving enhanced sensitivity compared to the Ni analog. In any case, the magnetically driven transition in $[(CH_3)_2NH_2]Co(HCOO)_3$ still relies upon formate distortions, a natural consequence of the superexchange ligand linking the metal centers.

CONCLUSION

To summarize, we combined magnetization, magneto-infrared spectroscopy, and lattice dynamics calculations to unveil the magnetic field-temperature phase diagrams in multiferroic $[(CH_3)_2NH_2]M(HCOO)_3$ (M = Mn^{2+}, Co^{2+}, Ni^{2+}). Although the magnetic saturation field of the Mn analog is experimentally realizable at 15.3 T, much higher fields are required to saturate the Ni and Co complexes. Both the magnetization data to 65 T and knowledge of the exchange energies suggest that these values are around 125 and 88 T, respectively. Analysis of the infrared spectrum of the Mn and Ni compounds across T_C reveals doublet splitting of the formate bending mode. This local lattice distortion is an order parameter of the ferroelectric transition. Interestingly, a power law fit shows that the dimensionality of these analogs develops differently through T_C, with $[(CH_3)_2NH_2]Ni(HCOO)_3$ being much more mean field like than $[(CH_3)_2NH_2]Mn(HCOO)_3$ as evidenced by the value of the critical exponent. By contrast, $[(CH_3)_2NH_2]Co(HCOO)_3$ reveals a surprising framework rigidity across the order–disorder transition due to modest distortions around the Co^{2+} centers. We therefore conclude that the transition to the ferroelectric state is driven solely by counterion freezing and the consequent hydrogen bonding. Under applied field in the Mn (and most likely, the Ni) compounds, the formate bending mode is involved in the transition to the fully saturated magnetic states, whereas the Co complex adopts a different mechanism involving formate stretching distortions. B-site substitution is thus a powerful tool for the development of structure–property relations within chemically analogous materials, providing control of electronic and magnetic properties as well as energy scales, without altering the overall architecture.

■ AUTHOR INFORMATION

Corresponding Author

*E-mail: musfeldt@utk.edu.

ORCID ⊕

Naresh S. Dalal: 0000-0002-9996-6918

Janice L. Musfeldt: 0000-0002-6241-823X

Notes

The authors declare no competing financial interest.

■ ACKNOWLEDGMENTS

■ REFERENCES

(1) Cheong, S.-W.; Mostovoy, M. Multiferroics: a magnetic twist for ferroelectricity. *Nat. Mater.* **2007**, *6*, 13−20.

(2) Vaz, C. A. F.; Hoffman, J.; Ahn, C. H.; Ramesh, R. Magnetoelectric coupling effects in multiferroic complex oxide composite structures. *Adv. Mater.* **2010**, *22*, 2900−2918.

(3) Spaldin, N. A.; Fiebig, M. The renaissance of magnetoelectric multiferroics. *Science* **2005**, *309*, 391−392.

(4) Khomskii, D. Classifying multiferroics: mechanisms and effects. *Physics* **2009**, *2*, 20.

(5) Mittal, S. A survey of techniques for architecting processor components using domain-wall memory. *ACM J. Emerg. Technol. Comput. Syst.* **2017**, *13*, 1−25.

(6) Ramesh, R.; Spaldin, N. A. Multiferroics: progress and prospects in thin films. *Nat. Mater.* **2007**, *6*, 21−29.

(7) Lee, J. H.; et al. A strong ferroelectric ferromagnet created by means of spin-lattice coupling. *Nature* **2010**, *466*, 954−958.

(8) Lorenz, B. Hexagonal manganites-($RMnO_3$): Class (I) multiferroics with strong coupling of magnetism and ferroelectricity. *ISRN Condens. Matter Phys.* **2013**, *2013*, 497073.

(9) Mundy, J. A.; et al. Atomically engineered ferroic layers yield a room-temperature magnetoelectric multiferroic. *Nature* **2016**, *537*, 523−527.

(10) Polyakov, A. O.; Arkenbout, A. H.; Baas, J.; Blake, G. R.; Meetsma, A.; Caretta, A.; Van Loosdrecht, P. H. M.; Palstra, T. T. M. Coexisting ferromagnetic and ferroelectric order in a $CuCl_4$-based organic-inorganic hybrid. *Chem. Mater.* **2012**, *24*, 133−139.

(11) Cai, H. L.; Zhang, Y.; Fu, D. W.; Zhang, W.; Liu, T.; Yoshikawa, H.; Awaga, K.; Xiong, R. G. Above-room-temperature magnetodielectric coupling in a possible molecule-based multiferroic: triethylmethylammonium tetrabromoferrate(III). *J. Am. Chem. Soc.* **2012**, *134*, 18487−18490.

(12) Tian, Y.; Stroppa, A.; Chai, Y.; Yan, L.; Wang, S.; Barone, P.; Picozzi, S.; Sun, Y. Cross coupling between electric and magnetic orders in a multiferroic metal-organic framework. *Sci. Rep.* **2015**, *4*, 1−5.

(13) Clune, A.; Hughey, K.; Lee, C.; Abhyankar, N.; Ding, X.; Dalal, N.; Whangbo, M.-H.; Singleton, J.; Musfeldt, J. Magnetic field-temperature phase diagram of multiferroic $[(CH_3)_2NH_2]Mn$-$(HCOO)_3$. *Phys. Rev. B: Condens. Matter Mater. Phys.* **2017**, *96*, 104424.

(14) Gómez-Aguirre, L. C.; Pato-Doldón, B.; Mira, J.; Castro-García, S.; Señarís Rodríguez, M. A.; Sanchez-Andújar, M.; Singleton, J.; Zapf, V. S. Magnetic ordering-induced multiferroic behavior in $[CH_3NH_3]$-$[Co(HCOO)_3]$ metal-organic framework. *J. Am. Chem. Soc.* **2016**, *138*, 1122−1125.

(15) Ptak, M.; Mączka, M.; Gągor, A.; Sieradzki, A.; Stroppa, A.; Di Sante, D.; Perez-Mato, J. M.; Macalik, L. Experimental and theoretical studies of structural phase transition in a novel polar perovskite-like $[C_2H_5NH_3][Na_{0.5}Fe_{0.5}(HCOO)_3]$ formate. *Dalt. Trans.* **2016**, *45*, 2574−2583.

(16) Ackermann, M.; Lorenz, T.; Becker, P.; Bohatý, L. Magneto-electric properties of $A_2[FeCl_5(H_2O)]$ with A = K, Rb, Cs. *J. Phys.: Condens. Matter* **2014**, *26*, 506002.

(17) Lunkenheimer, P.; Müller, J.; Krohns, S.; Schrettle, F.; Loidl, A.; Hartmann, B.; Rommel, R.; De Souza, M.; Hotta, C.; Schlueter, J. A.; Lang, M. Multiferroicity in an organic charge-transfer salt that is suggestive of electric-dipole-driven magnetism. *Nat. Mater.* **2012**, *11*, 755−758.

(18) Huang, C.; Du, Y.; Wu, H.; Xiang, H.; Deng, K.; Kan, E. Discovery of intrinsic ferromagnetic ferroelectricity in transition metal halides monolayer. *Phys. Rev. Lett.* **2018**, *120*, 147601.

(19) Baker, P. J.; Lancaster, T.; Franke, I.; Hayes, W.; Blundell, S. J.; Pratt, F. L.; Jain, P.; Wang, Z.-M.; Kurmoo, M. Muon spin relaxation investigation of magnetic ordering in the hybrid organic-inorganic perovskites $[(CH_3)_2NH_2]M(HCOO)_3$ (M = Ni,Co,Mn,Cu). *Phys. Rev. B: Condens. Matter Mater. Phys.* **2010**, *82*, 012407.

(20) Jain, P.; Ramachandran, V.; Clark, R. J.; Zhou, H. D.; Toby, B. H.; Dalal, N. S.; Kroto, H. W.; Cheetham, A. K. Multiferroic behavior associated with an order-disorder hydrogen bonding transition in metal-organic frameworks (MOFs) with the perovskite ABX_3 architecture. *J. Am. Chem. Soc.* **2009**, *131*, 13625−13627.

(21) Wang, Y. P.; Li, X. G.; Zhang, X. G.; Christou, G.; Cheng, H. P. Cation substitution effect on a molecular analogue of perovskite manganites. *J. Phys. Chem. C* **2017**, *121*, 10893−10898.

(22) Ackermann, M.; Brüning, D.; Lorenz, T.; Becker, P.; Bohatý, L. Thermodynamic properties of the new multiferroic material $(NH_4)_2[FeCl_5(H_2O)]$. *New J. Phys.* **2013**, *15*, 123001.

(23) Xu, K.; Lu, X.-Z.; Xiang, H. Designing new ferroelectrics with a general strategy. *npj Quantum Mater.* **2017**, *2*, 1.

(24) Mączka, M.; Gągor, A.; Macalik, B.; Pikul, A.; Ptak, M.; Hanuza, J. Order-disorder transition and weak ferromagnetism in the perovskite metal formate frameworks of $[(CH_3)_2NH_2][M(HCOO)_3]$ and $[(CH_3)_2ND_2][M(HCOO)_3]$ (M = Ni, Mn). *Inorg. Chem.* **2014**, *53*, 457−467.

(25) Yadav, R.; Swain, D.; Bhat, H. L.; Elizabeth, S. Order-disorder phase transition and multiferroic behaviour in a metal organic framework compound $(CH_3)_2NH_2Co(HCOO)_3$. *J. Appl. Phys.* **2016**, *119*, 064103.

(26) Wang, X. Y.; Gan, L.; Zhang, S. W.; Gao, S. Perovskite-like metal formates with weak ferromagnetism and as precursors to amorphous materials. *Inorg. Chem.* **2004**, *43*, 4615−4625.

(27) Duncan, H. D.; Dove, M. T.; Keen, D. A.; Phillips, A. E. Local structure of the metal-organic perovskite dimethylammonium manganese(II) formate. *Dalt. Trans.* **2016**, *45*, 4380−4391.

(28) Jain, P.; Stroppa, A.; Nabok, D.; Marino, A.; Rubano, A.; Paparo, D.; Matsubara, M.; Nakotte, H.; Fiebig, M.; Picozzi, S.; Choi, E. S.; Cheetham, A. K.; Draxl, C.; Dalal, N. S.; Zapf, V. S. Switchable electric polarization and ferroelectric domains in a metal-organic-framework. *npj Quantum Mater.* **2016**, *1*, 16012.

(29) Wang, W.; Yan, L. Q.; Cong, J. Z.; Zhao, Y. L.; Wang, F.; Shen, S. P.; Zou, T.; Zhang, D.; Wang, S. G.; Han, X. F.; Sun, Y. Magnetoelectric coupling in the paramagnetic state of a metal-organic framework. *Sci. Rep.* **2013**, *3*, 2024.

(30) Abhyankar, N.; Bertaina, S.; Dalal, N. S. On Mn^{2+} EPR probing of the ferroelectric transition and absence of magnetoelectric coupling in dimethylammonium manganese formate $(CH_3)_2NH_2Mn$-$(HCOO)_3$, a metal-organic complex with the Pb-free perovskite framework. *J. Phys. Chem. C* **2015**, *119*, 28143−28147.

(31) Vinod, K.; Deepak, C. S.; Sharma, S.; Sornadurai, D.; Satya, A. T.; Ravindran, T. R.; Sundar, C. S.; Bharathi, A. Magnetic behavior of the metal organic framework $[(CH_3)_2 NH_2]Co(HCOO)_3$. *RSC Adv.* **2015**, *5*, 37818−37822.

(32) López-Beceiro, J.; Gracia-Fernández, C.; Gómez-Barreiro, S.; Castro-García, S.; Sánchez-Andújar, M.; Artiaga, R. Kinetic study of the low-temperature transformation of $Co(HCOO)_3[(CH_3)_2NH_2]$. *J. Phys. Chem. C* **2012**, *116*, 1219−1224.

(33) Mączka, M.; Pietraszko, A.; Macalik, L.; Sieradzki, A.; Trzmiel, J.; Pikul, A. Synthesis and order-disorder transition in a novel metal formate framework of $[(CH_3)_2NH_2\text{-}Na_{0.5}Fe_{0.5}(HCOO)_3]$. *Dalt. Trans.* **2014**, *43*, 17075−17084.

(34) Brinzari, T. V.; Chen, P.; Tung, L. C.; Kim, Y.; Smirnov, D.; Singleton, J.; Miller, J. S.; Musfeldt, J. L. Magnetoelastic coupling in $[Ru_2(O_2CMe)_4]_3[Cr(CN)_6]$ molecule-based magnet. *Phys. Rev. B: Condens. Matter Mater. Phys.* **2012**, *86*, 214411.

(35) Hughey, K. D.; Clune, A. J.; Yokosuk, M. O.; Al-Wahish, A.; O'Neal, K. R.; Fan, S.; Abhyankar, N.; Xiang, H.; Li, Z.; Singleton, J.; Dalal, N. S.; Musfeldt, J. L. Phonon mode links ferroicities in multiferroic $[(CH_3)_2NH_2]Mn(HCOO)_3$. *Phys. Rev. B: Condens. Matter Mater. Phys.* **2017**, *96*, 180305.

(36) Liechtenstein, A. I.; Anisimov, V. I.; Zaanen, J. Density-functional theory and strong interactions: Orbital ordering in Mott-Hubbard insulators. *Phys. Rev. B: Condens. Matter Mater. Phys.* **1995**, *52*, R5467−R5471.

(37) Perdew, J.; Burke, K.; Ernzerhof, M. Generalized gradient approximation made simple. *Phys. Rev. Lett.* **1996**, *77*, 3865−3868.

(38) Kresse, G.; Furthmüller, J. Efficient iterative schemes for ab initio total-energy calculations using a plane-wave basis set. *Phys. Rev. B: Condens. Matter Mater. Phys.* **1996**, *54*, 11169−11186.

(39) Kresse, G.; Furthmüller, J. Efficient iterative schemes for ab initio total-energy calculations using a plane-wave basis set. *Phys. Rev. B: Condens. Matter Mater. Phys.* **1996**, *54*, 11169−11186.

(40) Zhang, Q.; Li, B.; Chen, L. First-principles study of microporous magnets M-MOF-74 (M = Ni, Co, Fe, Mn): The role of metal centers. *Inorg. Chem.* **2013**, *52*, 9356−9362.

(41) Blöchl, G.; et al. Projector augmented-wave method. *Phys. Rev. B: Condens. Matter Mater. Phys.* **1994**, *50*, 17953−17979.

(42) Kresse, G.; Joubert, D. From ultrasoft pseudopotentials to the projector augmented-wave method. *Phys. Rev. B: Condens. Matter Mater. Phys.* **1999**, *59*, 1758−1775.

(43) This data was benchmarked with a vibrating sample magnetometer.

(44) Casto, L. D.; Clune, A. J.; Yokosuk, M. O.; Musfeldt, J. L.; Williams, T. J.; Zhuang, H. L.; Lin, M. W.; Xiao, K.; Hennig, R. G.; Sales, B. C.; Yan, J. Q.; Mandrus, D. Strong spin-lattice coupling in $CrSiTe_3$. *APL Mater.* **2015**, *3*, 041515.

(45) Clune, A. J.; Hughey, K. D.; Lee, M.; Nam, J.; Tian, W.; Fernandez Baca, J.; Singleton, J.; Lee, J.-H.; Musfeldt, J. L., in preparation.

(46) Brinzari, T. V.; Chen, P.; Sun, Q. C.; Liu, J.; Tung, L. C.; Wang, Y.; Schlueter, J. A.; Singleton, J.; Manson, J. L.; Whangbo, M. H.; Litvinchuk, A. P.; Musfeldt, J. L. Quantum critical transition amplifies magnetoelastic coupling in $Mn[N(CN)_2]_2$. *Phys. Rev. Lett.* **2013**, *110*, 237202.

(47) At higher temperatures, the broadened Co feature is too subtle to track within the noise level.

(48) Goodenough, J. B. In *Magnetism and the Chemical Bond*; Cotton, F. A., Ed.; John Wiley & Sons, Inc.: New York, 1963.

(49) Brinzari, T. V.; Haraldsen, J. T.; Chen, P.; Sun, Q. C.; Kim, Y.; Tung, L. C.; Litvinchuk, A. P.; Schlueter, J. A.; Smirnov, D.; Manson, J. L.; Singleton, J.; Musfeldt, J. L. Electron-phonon and magnetoelastic interactions in ferromagnetic $Co[N(CN)_2]_2$. *Phys. Rev. Lett.* **2013**, *111*, 1−5.

(50) Sánchez-Andújar, M.; Gómez-Aguirre, L. C.; Pato Doldán, B.; Yáñez-Vilar, S.; Artiaga, R.; Llamas-Saiz, A. L.; Manna, R. S.; Schnelle, F.; Lang, M.; Ritter, F.; Haghighirad, A. A.; Señarís Rodríguez, M. A. First-order structural transition in the multiferroic perovskite-like

formate $[(CH_3)_2NH_2][Mn(HCOO)_3]$. *CrystEngComm* **2014**, *16*, 3558−3566.

(51) Mączka, M.; Zierkiewicz, W.; Michalska, D.; Hanuza, J. Vibrational properties and DFT calculations of the perovskite metal formate framework of $[(CH_3)_2NH_2[Ni(HCOO_3)]$ system. *Spectrochim. Acta, Part A* **2014**, *128*, 674−680.

(52) Mączka, M.; da Silva, T. A.; Paraguassu, W.; Ptak, M.; Hermanowicz, K. Raman and IR studies of pressure- and temperature-induced phase transitions in $[(CH_2)_3NH_2][Zn(HCOO)_3]$. *Inorg. Chem.* **2014**, *53*, 12650−12657.

(53) Ciupa, A.; Mączka, M.; Gągor, A.; Sieradzki, A.; Trzmiel, J.; Pikul, A.; Ptak, M. Temperature-dependent studies of $[(CH_3)_2NH_2]\text{-}[Fe^{III}M^{II}(HCOO)_6]$ frameworks (M^{II} = Fe and Mg): structural, magnetic, dielectric and phonon properties. *Dalt. Trans.* **2015**, *44*, 8846−8854.

(54) Szymborska-Malek, K.; Trzebiatowska-Gusowska, M.; Mączka, M.; Gągor, A. Temperature-dependent IR and Raman studies of metal-organic frameworks $[(CH_3)_2NH_2][M(HCOO)_3]$, M = Mg and Cd. *Spectrochim. Acta, Part A* **2016**, *159*, 35−41.

(55) Xin, L.; Fan, Z.; Li, G.; Zhang, M.; Han, Y.; Wang, J.; Ong, K. P.; Qin, L.; Zheng, Y.; Lou, X. Growth of centimeter-sized $[(CH_3)_2NH_2][Mn(HCOO)_3]$ hybrid formate perovskite single crystals and Raman evidence of pressure-induced phase transitions. *New J. Chem.* **2017**, *41*, 151−159.

(56) Blundell, S. *Magnetism in Condensed Matter*; Oxford University Press: Oxford, 2001.

(57) Kagawa, F.; Miyagawa, K.; Kanoda, K. Unconventional critical behaviour in a quasi-two-dimensional organic conductor. *Nature* **2005**, *436*, 534−537.

(58) Al-Wahish, A.; O'Neal, K. R.; Lee, C.; Fan, S.; Hughey, K.; Yokosuk, M. O.; Clune, A. J.; Li, Z.; Schlueter, J. A.; Manson, J. L.; Whangbo, M.-H.; Musfeldt, J. L. Magnetic phase transitions and magnetoelastic coupling in S = 1/2 Heisenberg antiferromagnets. *Phys. Rev. B: Condens. Matter Mater. Phys.* **2017**, *95*, 104437.